PHYSICAL REVIEW E VOLUME 62, NUMBER 6 DECEMBER 2000

Tubular plasma generation with a high-power hollow Bessel beam

J. Fan, E. Parra, I. Alexeev, K. Y. Kim, and H. M. Milchberg
Institute for Physical Science and Technology, University of Maryland, College Park, Maryland 20742

L. Ya. Margolin and L. N. Pyatnitskii
Institute for High Temperatures, Russian Academy of Sciences, Izhorskaya ulica 13/19, 127412 Moscow, Russia

(Received 23 August 2000; revised manuscript received September 25 2000)

A high power, hollow Bessel beam (J_5) is generated using an axicon and a phase plate in combination. The optical breakdown of a gas target and generation of a tubular plasma fiber with such a beam is realized. Hydrodynamic simulations of the hollow beam-plasma breakdown and heating are in reasonable agreement with interferometric measurements of the plasma time evolution.

PACS number(s): 52.40.Nk, 52.50.Jm

Hollow optical beams, those with maximum intensity located radially away from the optical axis, have attracted recent interest. Such beams have been used to guide and transport atoms using the polarization gradient force [1], pondermotively trap high energy electrons [2], and have been proposed for inducing cylindrical compression of fast ions induced by radially directed ponderomotive forces [3].

In this Rapid Communication, we use an intense hollow laser beam to break down a gas to form a tubular plasma, with maximum electron density initially located radially away from the optical axis. Since the index of refraction of such a tubular plasma decreases with radius from the optical axis, it can be used as a waveguide for high intensity laser pulses. Such waveguides have applications to laser-based electron acceleration [4] or x-ray generation [5]. In our previous work, laser-produced plasma waveguides have been generated using zero order Bessel beams (J_0) with an intensity maximum on axis, which produces a plasma with an initial electron density maximum on axis. Subsequent shock wave generation at the radially expanding plasma periphery results in a hollow density profile [6]. The time scale for the initial generation of the shock wave is ~100 ps, consistent with the time over which ion-ion collisions can cause a radial mass density buildup in a subatmospheric density gas target. A hollow density profile sufficiently deep for strongly bound optical guiding develops several nanoseconds after the laser pulse, as the shock propagates radially outward [6,7].

In the present experiment, the plasma is generated with a fifth order Bessel beam (J_5), which has an intensity maximum radially off-axis. We measure prompt generation of electron density in the high intensity locations of the beam, at times before significant ion mass motion can occur. This makes possible the generation of plasma waveguides with much smaller effective core diameters than those produced through shock expansion. The results shown here constitute the smallest core diameter plasma waveguides produced to date by this method. Earlier work by some of us using J_5 beams produced with 5 ns pulses resulted in plasmas in which it was difficult to observe hollow electron density profiles [8]. For such long pump pulses, plasma hydrodynamic evolution ensures that the on-axis density depression will not survive beyond the earliest times in the pulse.

There are two main methods for generating hollow Bessel beams [9,10]. The most straightforward method uses a phase screw followed by an axicon. The phase screw is an optical plate whose thickness is constant with radius but increases linearly with azimuthal angle φ about the optical axis. A planar phase front passing through a phase screw picks up an azimuthally dependent phase $\Phi(\varphi)=k(n_p-1)(d/2\pi)\varphi = s\varphi$, where k is the wave number in the medium outside the phase screw, d is the maximum thickness of the screw, n_p is the refractive index of the screw plate material, and s is called the phase screw parameter. If $s=m$, where m is a positive integer, then this parameter plays the role of an azimuthal mode index. An axicon is a cone shaped lens, which converts a plane wave into a conical beam, where the incident beam's rays are redirected toward the optical axis at an angle γ and an extended focus is formed [11]. Following the phase screw plate by an axicon adds a radial phase shift, so that the total transverse phase factor imposed on the beam immediately after these elements is $\exp(i\Phi)$, where $\Phi(\rho,\varphi) = -k_{\perp,\mathrm{axicon}}\rho + s\varphi$, where ρ is the radial coordinate with respect to optical axis, $k_{\perp,\mathrm{axicon}}=\mathrm{k}\sin\gamma$, $\gamma=\sin^{-1}(n_a\sin\alpha) - \alpha$ is the angle between the focused axicon rays and the optical axis, α is the axicon cone base angle, and n_a is the refractive index of the axicon material. A hollow Bessel beam of order $m(J_m)$, for $s=m$, results from propagating this beam to the focal region of the axicon, as will be discussed below.

In the second method, a discrete approximation of the transverse phase Φ, combining the functions of both the phase screw and axicon, can be attained by using a transparent plate with an etched surface microrelief [10]. For use with high power laser pulses, the discrete phase plate was easier to fabricate than the continuous phase screw, so this method was used in the experiments described here. Here, the plate consisted of $N\times N$ radial and azimuthal segments ($i=1,\ldots,N$ and $j=1,\ldots,N$, where $N=3000$). For $2\pi n < -k_{\perp,\mathrm{plate}}\rho_{ij} + m\varphi_{ij} < 2\pi n + \pi$, the depth of the microrelief features was set to give $\Phi_{ij}=0$, and for $2\pi n+\pi < -k_{\perp,\mathrm{plate}}\rho_{ij} + m\varphi_{ij} < 2\pi n + 2\pi$, it was set to give $\Phi_{ij} = \pi$ (where n is a positive or negative integer). Here $k_{\perp,\mathrm{plate}}=k\sin\gamma_{\mathrm{plate}}$, where γ_{plate} is the angle of the rays with respect to the optical axis focused by the discrete phase plate. The hollow Bessel beam was formed by the phase

plate (with $m=5$, and $\gamma_{\text{plate}}=1°$) closely followed by an axicon (with $\alpha=30°$), giving an effective $\gamma=19°$. Since $k_{\perp,\text{plate}}/k_{\perp,\text{axicon}} \ll 1$, the phase plate acted mainly as an azimuthal phase screw, with most of the radial phase shift provided by the axicon.

Consider a linearly polarized laser beam $E_i(\rho)\hat{x}$ normally incident on an $m=5$ phase plate followed by an axicon, where $\hat{x}$ is the polarization unit vector, ρ is the radial coordinate in the incident beam, and the unit vector $\hat{z}$ is along the optical axis. Applying Kirchhoff's integral to the source amplitude and phase distribution just beyond the axicon, $E_i(\rho)\exp(i\Phi)\hat{x}$, and using the stationary phase approximation, gives the following squared magnitudes of the field components in the paraxial region ($r<z\sin\gamma$, $kr^2<z$) of the focus:

$$|E_x(r,z)|^2=\frac{\pi}{32}\frac{kz\sin^2\gamma}{\cos\gamma-\sin\gamma\tan\alpha}\left(1+\frac{1}{\cos(\alpha+\gamma)}\right)^2 E_i^2(\rho)\times\left\{(1+\cos\gamma)J_5(x)+\frac{1}{2}(1-\cos\gamma)\times[J_7(x)+J_3(x)]\right\}^2, \quad (1)$$

$$|E_z(r,z)|^2=\frac{\pi}{32}\frac{kz\sin^4\gamma}{\cos\gamma-\sin\gamma\tan\alpha}\left(1+\frac{1}{\cos(\alpha+\gamma)}\right)^2\times E_i^2(\rho)[J_4(x)-J_6(x)]^2.$$

Here r is the radius in the focal plane, and $J_m(x)$ is the mth order Bessel function, where $x=kr\sin\gamma$. If $z=0$ is located at the vertex of the axicon, then radial locations ρ of the incident beam are directed to axial locations z given by $\rho=z\tan\gamma/(1-\tan\alpha\tan\gamma)$. For $r=0$, the intensity is zero so that a hollow beam is formed along the optical axis over a maximum length $z_0=\rho_0(1-\tan\alpha\tan\gamma)/\tan\gamma$, where ρ_0 is the incident beam radius. For $\sin^2\gamma \ll 1$ and $(1-\cos\gamma)\ll 1$, as is the case here, $|E_z(r,z)|\sim 0$ and the focal intensity distribution is approximately

$$I(r,z)=\frac{\pi}{32}\frac{kz\sin^2\gamma}{\cos\gamma-\sin\gamma\tan\alpha}\left(1+\frac{1}{\cos(\alpha+\gamma)}\right)^2 I_0(\rho)\times[(1+\cos\gamma)J_5(x)]^2, \quad (2)$$

where $I_0(\rho)$ is the radial intensity distribution of the incident laser beam. The first maximum of $J_5(x)$ occurs at $x\approx 6.43$, giving $r_0=6.43/k\sin\gamma$ as the radius of the hollow beam. For $\lambda=1064$ nm and $\gamma=19°$, $r_0\sim 3.3\,\mu$m

The experimental setup is shown in Fig. 1. Pulses (500 mJ, 100 ps, 1064 nm) from a 10 Hz neodynium-doped yttrium aluminum garnet (Nd:YAG) laser system [12] were directed to the $m=5$ phase plate and axicon combination to generate a plasma in an ambient gas of 700 torr argon. A focal plane image of the hollow beam and a centered lineout is shown in Fig. 2(a), taken at low energy using a 60X microscope objective. The measured radius for the first maximum is $\sim 4\ \mu$m, somewhat larger than in the $|J_5|^2$ theoretical result, for which an image and lineout is shown in Fig. 2(b) for $\lambda=1064$ nm and $\gamma=19°$. There

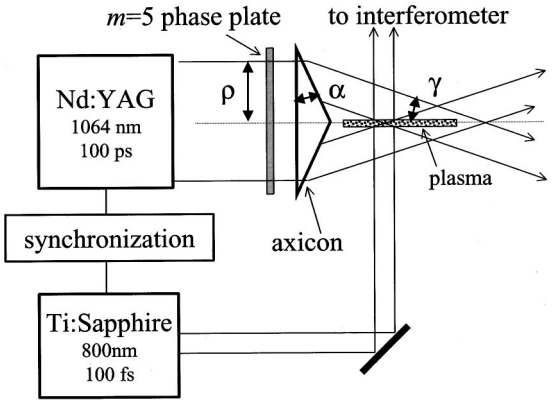

FIG. 1. Experimental arrangement, showing synchronization of Nd:YAG and Ti:sapphire laser systems, hollow beam optics, and interferometer setup.

was little distortion of the focal image when translating the microscope ~ 1 cm along the optical axis, and this was used as a test of the optical alignment accuracy. The peak intensity in the first ring was $\sim 2.5\times 10^{12}$ W/cm^2, more than an order of magnitude weaker than the peak intensity from the axicon without the phase plate. This results from the large area of the first ring compared to the central maximum of a J_0 beam.

The plasma generated by the hollow beam was ~ 0.8 cm long and uniform along the axis, with some tapering over ~ 1 mm at the ends. This was determined by scanning the interferometer viewing field along the full length of the plasma. To measure the time evolution of the plasma, a 100 fs, 800 nm, 1 mJ interferometer probe pulse was obtained from a separate Ti:sapphire laser synchronized to the Nd:YAG system with less than 10 ps of jitter. This synchronization is described in Ref. [13]. The probe pulse passed through an optical delay line (-200 ps to $+500$ ps with respect to the peak of the 1064 nm pump pulse) and was directed trans-

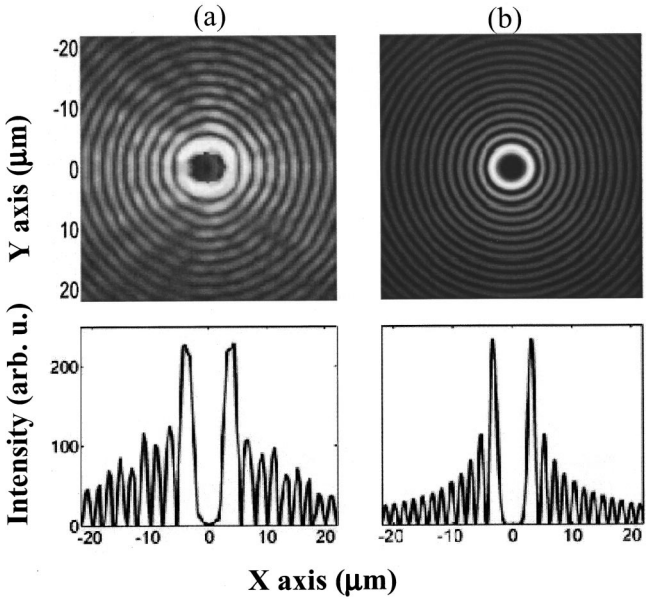

FIG. 2. (a) Image and lineout of focal region of $m=5$ phase plate and axicon combination for $\lambda=1064$ nm; (b) Theoretical plot and lineout for $|J_5|^2$ for $\gamma=19°$ and $\lambda=1064$ nm.

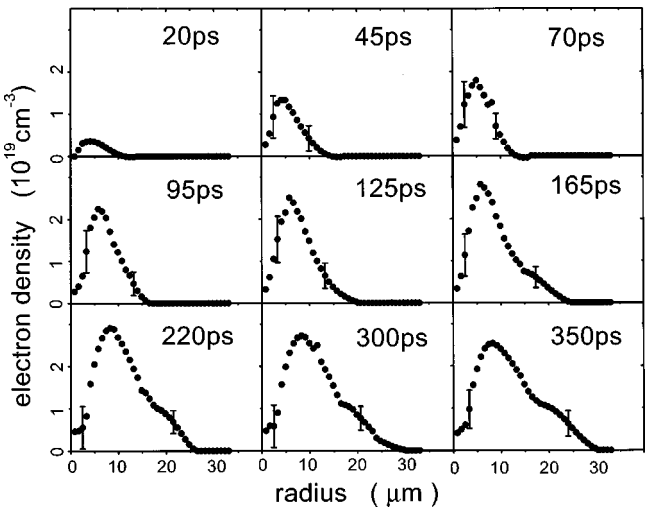

FIG. 3. Electron density profiles determined from interferometry. Pump pulse $\lambda=1064$ nm, 100 ps, peak intensity 2.5×10^{12} W/cm^2. The time $t=0$ corresponds to a peak electron density of 5×10^{17} cm^{-3}, representing the minimum detectable phase shift. The vertical bars represent the statistical standard deviation of profiles derived from individual phase lineouts.

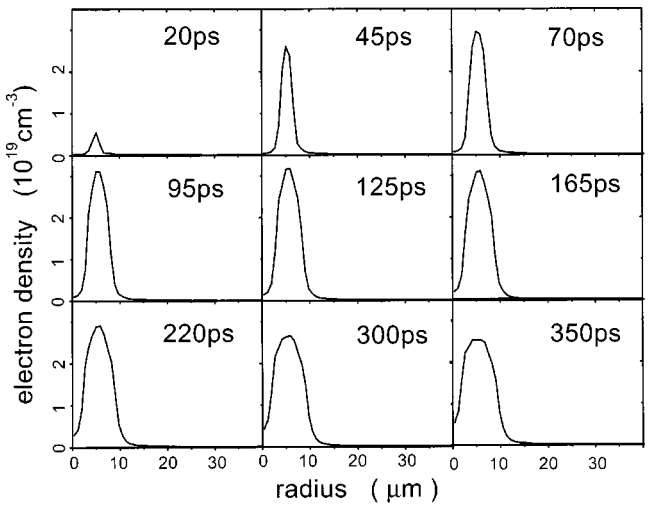

FIG. 4. Electron density profiles from simulation. The time $t=0$ is set from the appearance of a peak electron density of 5×10^{17} cm^{-3}.

versely across the plasma into an imaging Michelson interferometer. The interferogram phase was extracted using a fast Fourier transform technique and the electron density was determined through Abel inversion [6]. Electron density profiles from the central region of the plasma column for a number of delays are shown in Fig. 3. The zero time reference was assigned by the first appearance of a phase disturbance in the interferogram, at an electron density threshold of $\sim5\times10^{17}$ cm^{-3}. Each profile was obtained from averaging the extracted interferogram phase for ~200 μm along the optical axis, which was the extent of the field of view. It is seen that a hollow electron density profile clearly appears by 20 ps. The off-axis peak electron density continues to rise until it saturates by 170 ps at a level of $\sim3\times10^{19}$ cm^{-3}, at which point the pump pulse is well past its peak. From saturation out to 350 ps, the central part of the profile changes little except for a slight increase in the central density and a slight broadening at the radial periphery. Although we have not yet attempted to inject pulses into this waveguide, we calculate numerically [7] that the fundamental modes (which are wavelength independent [5]) are strongly bound with a nearly constant full width at half maximum (in intensity) of 3.1 μm for the electron density profiles between 95 and 350 ps. Compared to plasma waveguides generated with a J_0 Bessel beam, where the earliest time for very leaky quasi-bound guiding is ~120 ps after the channel peak density is generated [7,14], the waveguide generated with a J_5 Bessel beam can guide strongly bound modes at earlier times and at much smaller mode diameters.

The hollow Bessel beam-plasma interaction was simulated self-consistently [14] by coupling the radial wave equation for the hollow beam electric field, $d^2E/dr^2+(1/r)dE/dr+[\kappa^2(r)-m^2/r^2]\ E=0$, to a one-dimensional Lagrangian hydrocode, where $\kappa^2(r)=k^2[\sin^2\gamma+\delta_{\rm plasma}(r,\omega)+4\pi\chi(r,\omega)]$ is the effective transverse wave number, $k=\omega/c$ is the vacuum wave number, and $m(=5)$ is the azimuthal mode index. Here the plasma contribution to the refractive index is $\delta_{\rm plasma}(r,\omega)=-\xi+i\xi\nu/\omega$, where $\xi=(1+\nu^2/\omega^2)^{-1}N_e/N_{\rm cr}$, $N_e(r)$ is the electron density, $N_{\rm cr}=m\omega^2/4\pi e^2$ is the critical density, and $\nu(r)$ is the collision frequency, while $\chi(r,\omega)$ is the linear susceptibility of bound electrons in neutral atoms and ions. The calculation includes field ionization [15], collisional ionization, thermal conduction (both gradient-based and flux limited), and a collisional radiative model for the ionization dynamics. Starting with neutral gas, at each time step the above radial wave equation is solved using the plasma density profile of the previous time step, and the resulting electric field ionizes and heats the plasma, driving the hydrodynamics. [The theoretical profile of Fig. 2(b) was calculated by solving the radial wave equation for the vacuum case for $\gamma=19°$.] Figure 4 shows the electron density evolution calculated for the interaction with 700 torr of argon of a pulse with peak intensity of 2.5×10^{12} W/cm^2, $\lambda=1064$ nm, pulsewidth 100 ps, and $m=5$. An approach angle of $\gamma=15°$ rather than 19° was used so that in vacuum the first ring would be positioned to agree with the measurement of Fig. 2(a). The time $t=0$ was set by appearance of a peak density of 5×10^{17} cm^{-3}. By 20 ps a hollow profile with peak electron density of $\sim5\times10^{18}$ cm^{-3} has developed, and by 70 ps the peak off-axis density has saturated at $\sim3\times10^{19}$ cm^{-3}. At 700 torr, the ionization proceeds primarily through collisions (avalanche).

There are several differences between the measurements and the simulation. While the peak saturated densities and the central densities are in agreement, the saturation occurs faster in the simulation. This cannot be explained by a maximum probe pulse jitter of 10 ps, and at present we have no explanation. In addition, the simulation profiles are narrower in outer extent, and the location of the density peak remains almost stationary compared to the experimental profiles. This is likely a result of the wider main ring and the broader radial distribution of energy in the subsidiary rings of the experimental hollow beam [compare Figs. 2(a) and 2(b)], which would heat the outer region of the density profile to a higher temperature. The simulation predicts a peak temperature at the ring location of ~5 eV and a peak ionization of $Z=1$.

This explains the long time persistence of the central hole in the density profile, which fills in at about ~800 ps in the simulation. The temperature is too low for radially inward thermal conduction to quickly raise the ionization yield of the weakly ionized gas on axis or for rapid outward expansion of the channel. Even though the breakdown is in the avalanche regime, the low temperature and slow hydrodynamics is made possible by the modest peak intensity of $2.5\times10^{12}\,\mathrm{W/cm^2}$ of the 100 ps pulse. A similar result could be obtained using ultrashort pulses at much higher intensity in the field ionization regime [15], where the electron density would be strongly localized at the first ring and the residual electron temperature would be low [16].

In conclusion, we have demonstrated the generation of elongated, tubular plasmas using a high order Bessel beam. Some applications of this channel, such as guiding for laser-plasma accelerators, might be complicated by the remaining neutral gas on-axis, while others, such as harmonic generation, might benefit from its presence. In any case, the prompt generation of hollow, deep electron density profiles, without the need for hydrodynamic evolution to establish them, make possible the guiding of intense pulses of very small spot size.

This work is supported by the U.S. Department of Energy (Grant No. DEF G0297 ER 41039), the National Science Foundation (Grant No. PHY-9515509), and the Civilian Research and Development Foundation (CRDF Grant No. RP2-130).

[1] Y. Song, D. Milam, and W. T. Hill, Opt. Lett. **24**, 1805 (1999); J. Arlt, T. Hitomi, and K. Dholakia, Appl. Phys. B: Lasers Opt. **71**, 549 (2000).

[2] J. L. Chaloupka and D. D. Meyerhofer, Phys. Rev. Lett. **83**, 4538 (1999).

[3] G. S. Sarkisov, V. Yu. Bychenkov, and V. T. Tikhonchuk, Pisma Zh. Eksp. Teor. Fiz. **69**, 20 (1999) [JETP Lett. **69**, 20 (1999)].

[4] E. Esarey, P. Sprangle, Jonathan Krall, and A. Ting, IEEE Trans. Plasma Sci. **24**, 252 (1996).

[5] H. M. Milchberg, C. G. Durfee, and T. J. McIlrath, Phys. Rev. Lett. **25**, 2494 (1995); H. M. Milchberg, C. G. Durfee, and J. Lynch, J. Opt. Soc. Am. B **12**, 731 (1995).

[6] T. R. Clark and H. M. Milchberg, Phys. Rev. Lett. **78**, 2373 (1997).

[7] T. R. Clark and H. M. Milchberg, Phys. Rev. Lett. **81**, 357 (1998); Phys. Rev. E **61**, 1954 (2000).

[8] S. S. Bychkov, S. V. Gorlov, L. Ya. Margolin, L. N. Pyatnitskii, A. D. Tal'virskii, and G. V. Shpatakovskaya, Quantum Electron. **29**, 229 (1999).

[9] N. E. Andreev, L. Ya. Margolin, I. V. Pleshanov, and L. N. Pyatnitskii, Zh. Eksp. Teor. Fiz. **105**, 1232 (1994) [JETP **78**, 663 (1994)].

[10] N. E. Andreev, S. S. Bychkov, V. V. Kotlyar, L. Ya. Margolin, L. N. Pyatnitskii, and P. G. Serafimovitch, Quantum Electron. **26**, 126 (1996).

[11] F. V. Bunkin, V. V. Korobkin, Yu. A. Kurinyi, L. Ya. Polonsky, and L. N. Pyatnitsky, Kvantovaya Elektron. **10**, 443 (1983) [Sov. J. Quantum Electron. **13**, 254 (1983)].

[12] T. R. Clark, Ph.D. thesis, University of Maryland, College Park, 1998 (unpublished).

[13] S. P. Nikitin, T. M. Antonsen, T. R. Clark, Yulein Li, and H. M. Milchberg, Opt. Lett. **22**, 1787 (1997).

[14] J. Fan, E. Parra, and H. M. Milchberg, Phys. Rev. Lett. **84**, 3085 (2000).

[15] M. V. Ammosov, N. B. Delone, and V. P. Krainov, Zh. Eksp. Teor. Fiz. **91**, 2008 (1986) [JETP Lett. **64**, 1191 (1986)].

[16] B. M. Penetrante and J. N. Bardsley, Phys. Rev. A **43**, 3100 (1991).